

## THE USE OF OPTICAL ACTIVITY MEASUREMENTS IN OIL SHALE PROCESSING

Dale L. Lawlor\*, D. R. Latham\*, T. C. Bartke\*, and R. O. Asplund\*\*

\*Laramie Energy Research Center  
P. O. Box 3395  
Laramie, Wyo. 82071

\*\*University of Wyoming  
Chemistry Department  
Laramie, Wyo. 82071

### INTRODUCTION

Shale oil reserves are more than three and one-half times the amount of world petroleum reserves (1). But because of overburden, most of the reserves cannot be mined conventionally; an in-situ process must be used for oil recovery. The in-situ process has advantages over aboveground, conventional processes because transporting or crushing the shale is unnecessary before retorting; and spent shale disposal is no problem after retorting. But a disadvantage is the difficulty of monitoring the relatively deep underground conversion changes. One developing method for following these changes is optical activity measurements on the shale oil during its production because we know the optical activity of shale oil decreases with increasing heating rate (2). Shale oil is optically active because oil shale contains optically active biological markers derived from life forms existing during the formation of the shale deposit (3). Known biological markers--steranes, diterpanes, gammacerane, and perhydro- $\beta$ -carotene--are reduction products from diagenesis of former living systems. Despite the rigors of heating, in most retorting systems these optically active molecules survive in sufficient quantities to allow their detection with a sensitive spectropolarimeter. These measurements show promise in studying large-scale field retorting systems.

This study at the Laramie Energy Research Center (LERC) shows examples of optical activity measurements in a controlled-state retort system, in the Site 9 in-situ field experiment, located at Rock Springs, Wyo., and in differing retorting systems using Green River, Antrim, and Moroccan oil shales.

### EXPERIMENTAL

Optical activity measurements were made on the saturate fraction from the shale oil and bitumen, as described in detail earlier (2). Briefly, 1/2 g of dried oil in a 50-ml beaker was dissolved in 20 ml of cyclohexane (Burdick and Jackson Laboratories, Inc.). The solution was cooled to 0°C in a circulating cold bath, and 10 ml of 15 percent phosphorous pentoxide in sulfuric acid was slowly added with stirring. Stirring was continued for 1 hour, then the mixture was transferred and centrifuged for 1/2 hour at 3000 RPM. The cyclohexane layer was drawn off, and the bottom layer was twice more mixed with 10 ml of cyclohexane and centrifuged. Then the combined solution was decolorized by passing it over 10 gm of "powdered" silica gel (Baker, 60-200 mesh), eluting with cyclohexane, and collecting the first 10 ml of solution. The solution was evaporated under nitrogen to 20 ml. The optical activity was determined on this solution in the ORD mode with a Jasco J-20 spectropolarimeter. Optical activity data were determined in the 300- to 600-nm wavelength range and the solution was evaporated to dryness to determine the total saturates. The optical activity data were calculated based upon the amount of total saturates.

Shale oils and bitumens from an interrupted, controlled-state retort experiment (4) were analyzed. Green River formation oil shale, 1/8-to 1/2-in. particle

size, was packed into a vertical 3-in. stainless steel pipe and was externally electrically heated in 6-in. increments at a 2°F-per-minute heating rate with a zone travel rate of 3 in. per hour. Produced oil flowed downward with assistance from a nitrogen sweep gas. After approximately half of the shale column had reached a temperature of 1000°F (about 36 hours), the experiment was stopped; the pipe was cooled with water and cut into 24 6-in. segments. The shale samples from the 24 segments consisted of 14 spent-shale samples and 10 samples of oil-wet shale, with varying temperature exposures from 730°F to ambient. The oil-wet shale samples were rinsed with cyclohexane to recover the surface oil samples. The rinsed samples were dried at room temperature, crushed to 200 mesh, and Soxhlet extracted for 48 hours with cyclohexane to obtain the bitumen samples. The surface oil and bitumen samples were prepared and analyzed for optical activity as described.

Optical activity analyses were made on several retorting systems using the described method. Nine composite samples of shale oil were analyzed, representing 6 months of operation at the LERC Site 9 in-situ field experiment (5). Shale oils were analyzed from the bench-scale controlled-state retort system; from five aboveground, semi-works retort systems; and from two large-block systems.

#### RESULTS AND DISCUSSION

Only data from the 450-nm wavelength are presented in Figures 1 and 2 for ease of interpretation. Shale oil optical activity changes as the retort heating rate changes (2). And since heating rate consists of two components, temperature and time, optical activity changes should be related to each of these components. Data from analysis of oils and bitumens from the interrupted controlled-state retort are shown in Figure 1. Oils rinsed from the surface of the cooler shale have, except for samples 15 and 24, a specific rotation of about 4 units. Sample 15, having been exposed to the hottest temperature (730°F), shows only a trace of activity; and the last sample, 24, has about nine degrees of rotation, possibly because the cooler end of the retort causes dilution by accumulations of saturates. The wavelike distribution of the data is probably real in that it is well within the testing limits. The receiver oil, from about one-half of the total charged shale, shows an optical rotation of about four degrees, approximating the values from the surface oils.

The optical activity of the bitumens extracted from the partly retorted shale (samples 15 to 19) and from the unretorted shale (samples 20 to 24) is also shown in Figure 1. A smooth curve evolves, proceeding from sample 20 to 15, indicating that the effect of heat on the shale produces a uniform loss of optical activity in the bitumen. An induction period before the retorting of the shale (estimated to occur at about 400°F) occurs in the low-temperature loss of activity in samples 19 to 17. Sample 19 has a rotation of approximately 12 degrees; number 17 approximately 10 degrees. This 2-degree difference apparently results from increasing the temperature from 110 to 190°F over a 4-hour period. Samples 15 and 16 reflect a rapid loss of activity as the shale becomes heated to retorting temperature with subsequent emergence of oil. The rapid increase in optical activity from sample 20 to 23 cannot be satisfactorily explained at this time but approaches the optical activity of Green River natural bitumen--typically 30 units.

Oils from the Site 9 in-situ field experiment were analyzed for optical activity. The results in Figure 2 show that the oils produced during the first part of the 6-month experiment were more optically active than those in the second half. The lower optical activity in the second half of the experiment probably results from a different thermal history. The results may reflect change in the air-injection system when on the 60th day the injection well was changed from well No. 1 (located at the center of the site) to well No. 10 (located nearer the edge of the site), thereby moving the air injection closer to the moving combustion front, possibly further decomposing previously accumulated oil. The general decrease in

optical activity for all the composite oils indicates that after 6 months of production a "steady state" oil was not produced. The general indication of oil decomposition is not evident in 10 other physical or chemical tests, as shown in Table 1. Traditional indications of oil thermal decomposition such as increasing olefin, aromatic, and naphtha contents or decreasing viscosity and pour point, are not unequivocally present. In some instances, as in olefin content, the last four samples are in opposition to the optical activity data by having generally lower amounts of olefins--less oil decomposition. The optical activity data indicate that the last four samples are decomposed the most.

TABLE 1. - Properties of Site 9 composite oils

Property	Sample number								
	1	2	3	4	5	6	7	8	9
Naphtha, percent*	9	6	6	8	10	10	11	12	14
Olefins, percent in naphtha	36	32	25	19	--	19	14	27	9
Olefins, percent in light distillate	22	37	38	35	--	15	13	12	33
Paraffins, percent in naphtha	43	17	51	57	--	54	59	45	63
Paraffins, percent in light distillate	22	46	49	52	49	52	57	56	38
Aromatics, percent in naphtha	21	22	24	24	--	27	27	28	28
Aromatics, percent in light distillate	35	17	13	13	34	33	30	32	29
Residuum, percent*	6	6	6	7	5	4	5	8	7
Viscosity, SUS 100°F	53	58	57	53	50	46	47	56	45
Pour point, °F	35	40	40	45	45	40	45	40	35
Optical activity $[\alpha]_{450}^{25}$	3.2	2.1	1.9	1.8	1.6	0.8	0.6	0.3	0.2

\*Determined by simulated distillation

Oils from different retorting systems were analyzed for optical activity to determine the possibility of observing basic differences among retorting systems. The results in Figure 3 show that differences are observable. Data from the entire 300- to 600-nm range are presented in Figures 3 and 4 for more comprehensive data evaluation. Generally, the optical activity data may be categorized into three groups. First, the least decomposed oils are derived from the controlled-state system where small shale particles, gravity flow, and nitrogen gas sweeping allowed the produced oil to escape from the shale easily thereby minimizing secondary oil decomposition. The second group of oils was produced from large, aboveground,

semi-works retorts with relatively medium shale particles (1 to 6 in.) and moderate capability for the oil to escape the shale. The third group of oils was produced from LERC's aboveground, simulated in-situ 150-ton retort and the Site 9 in-situ system that may be characterized as large-block systems; therefore, slow escape of oil from the shale would be probable. Slow escape of oil would presumably cause considerable decomposition.

Optical activity comparisons were made among oils produced in the LERC 10-ton retort using Green River, Antrim, and Moroccan shales. Figure 4 shows the Green River shale oil to be the most optically active by at least a factor of 2 at all wavelengths. The Antrim and Moroccan shale oils have essentially identical activity probably reflecting the amounts of optically active components in the original shales. These shales have, interestingly, a marine origin, while the Green River shale has a nonmarine origin.

#### SUMMARY

Optical activity measurements of shale oils allow insights into retorting conditions that are not observable by traditional analytical methods. With a bench-scale retort, a low-temperature induction period in the shale before retorting can be observed. The retorting phase itself may be observed by following changes in bitumen and in surface oil optical activity. Optical activity data from Site 9 composite oils, representing 6 months of production, reflect two distinct retorting phases of the experiment. The second, lower optically active phase, may have resulted from secondary degradation of previously accumulated oil. Despite 6 production months, a "steady state" oil was not produced. Optical activity data from 10 different retorting system oils show decreasing optical activity with increasing shale size.

#### REFERENCES

1. D. C. Duncan, Ind. Petrol. Assoc. Am., pp. 22, 49-51, Aug. 1958.
2. D. L. Lawlor, Preprints, Amer. Chem. Soc., Div. Fuel Chem., v. 22, (3), 100 (1977).
3. D. E. Anders and W. E. Robinson, Geochim. et Cosmochim. Acta, v. 35, 661 (1977).
4. J. J. Duvall and H. B. Jensen, Quart. Colo. School of Mines, v. 70, (3), 187 (1975).
5. A. Long, Jr., N. W. Merriam, and C. G. Mones, Ibid. (1977). (In press).

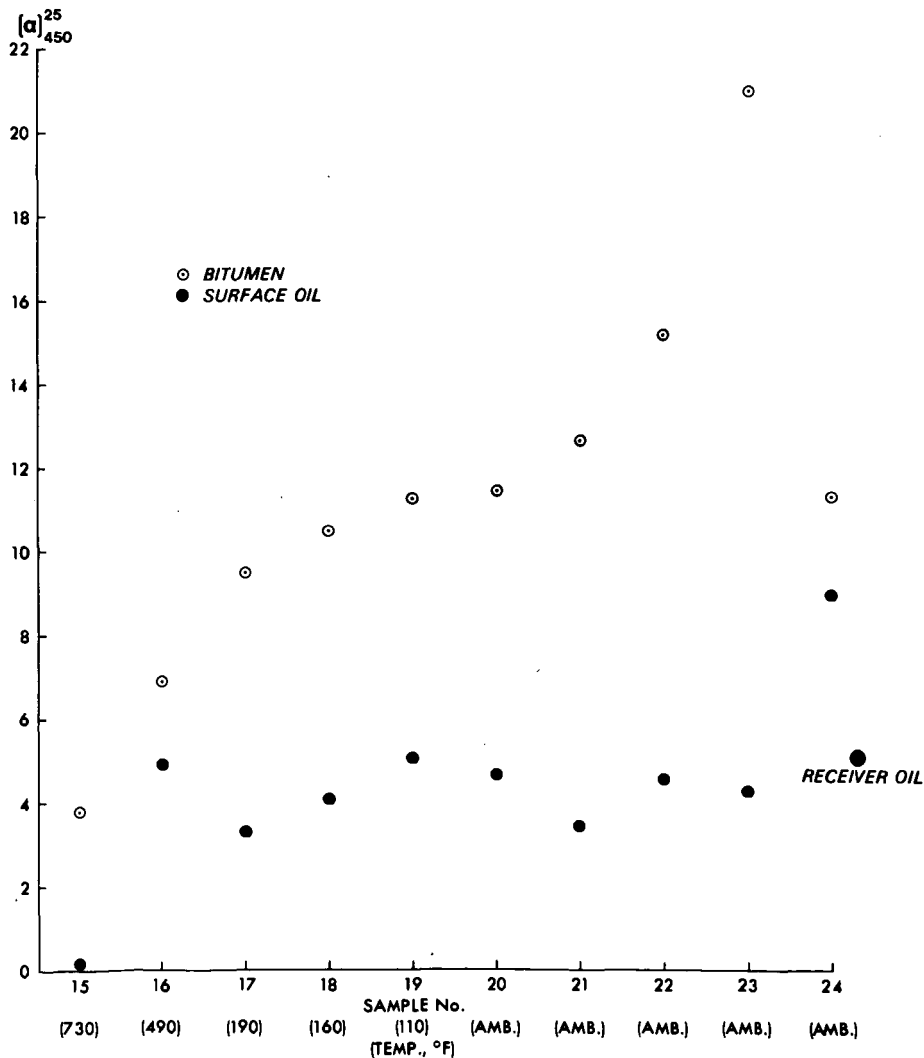


FIGURE 1. - OPTICAL ACTIVITY OF SATS. (450nm.).

INTERRUPTED CONTROLLED STATE RETORT.

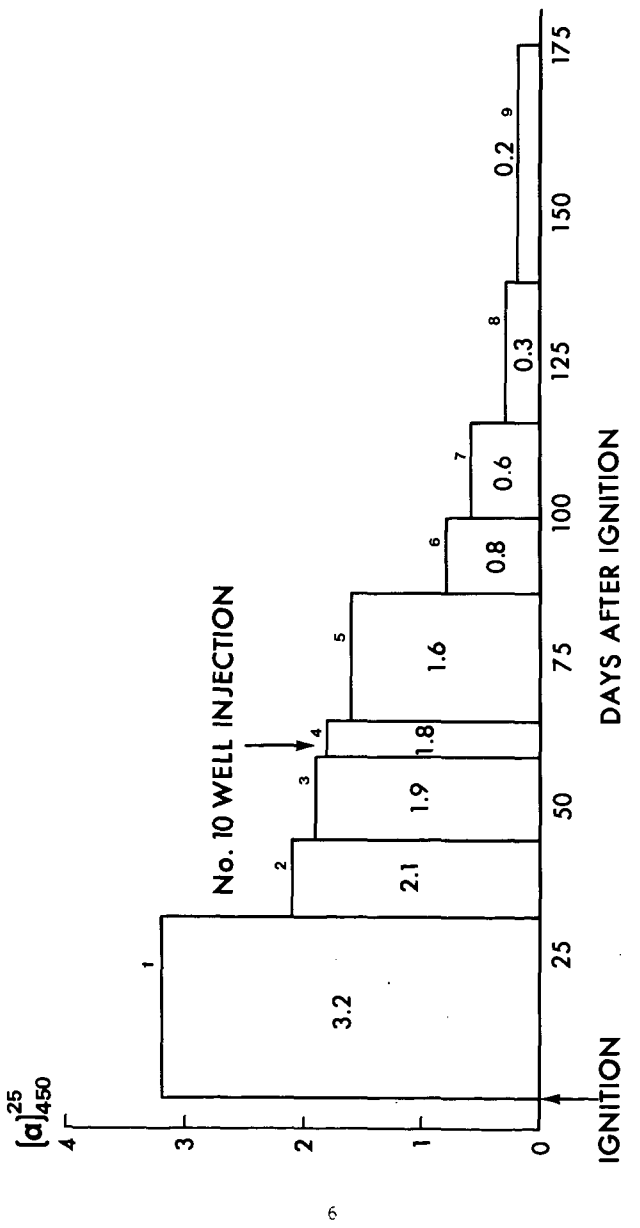
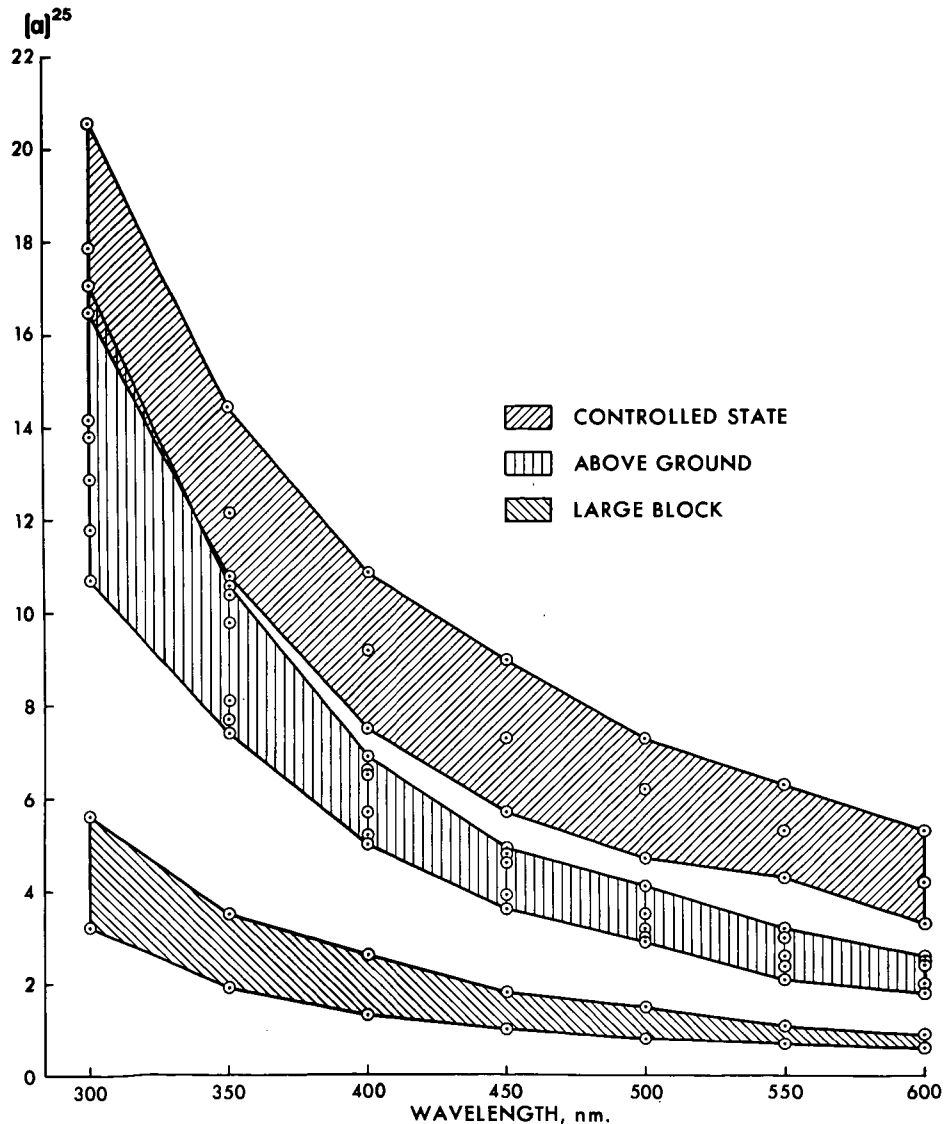


FIGURE 2. - OPTICAL ACTIVITY OF SITE 9 COMPOSITE OILS.



**FIGURE 3. - OPTICAL ACTIVITY OF OILS FROM DIFFERENT RETORTS,  
GREEN RIVER FORMATION SHALES.**

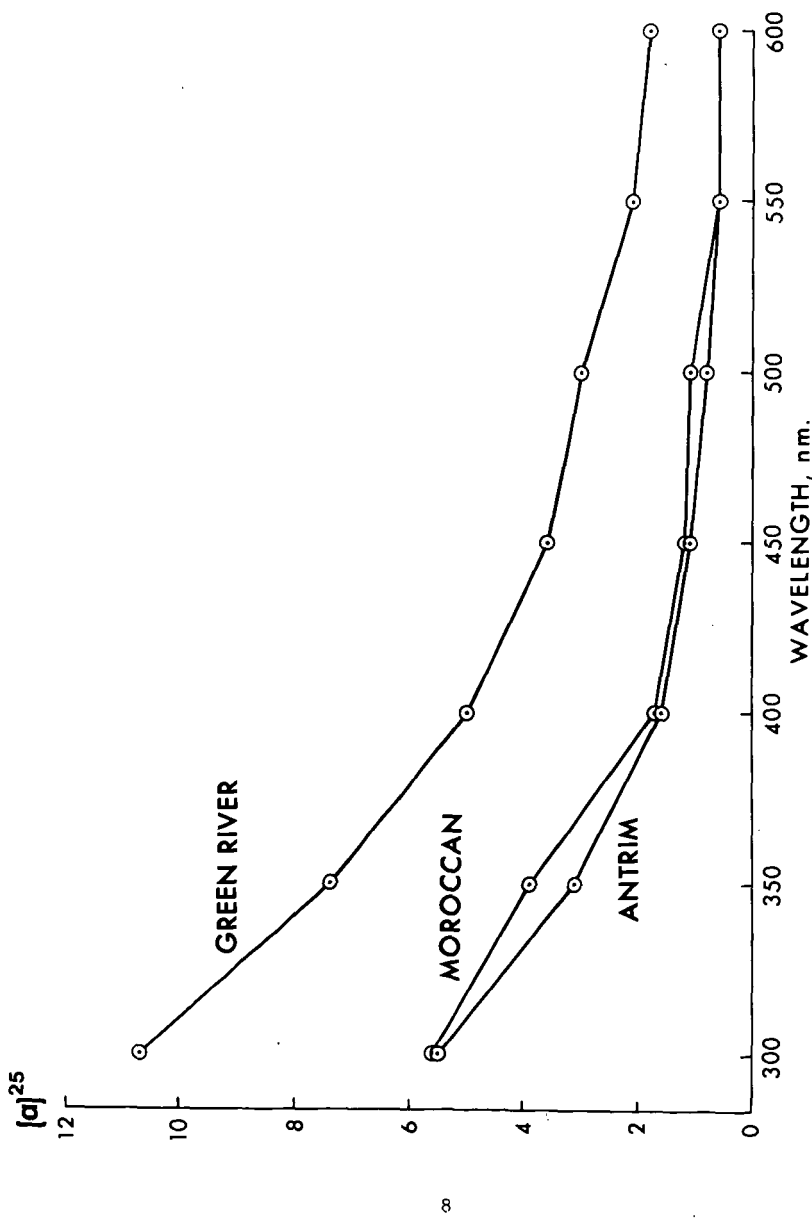


FIGURE 4. - OPTICAL ACTIVITY OF GREEN RIVER, ANTRIM AND  
MOROCCAN SHALE OILS, 10 TON RETORT.

PETROGRAPHIC METHOD FOR SELECTIVE DETERMINATION OF A COMPONENT  
(RAW COAL) IN A MIXTURE OF PRODUCTS FROM PROCESSING OF COAL

D. M. Mason

Y. Julian

Institute of Gas Technology  
3424 S. State Street  
Chicago, Illinois 60616

Introduction

In the HYGAS<sup>®</sup> pilot plant gasification reactor, fine particles from each reactor stage become entrained in the gas and are carried into the exit-gas cyclone and are removed from the gas. Thus, the dust removed by the pilot plant cyclone includes particles from the steam-oxygen-gasification fluidized bed, the second-stage hydrogasification fluidized bed, the first-stage hydrogasification entrained reactor, and the slurry drier fluidized bed. (See Figure 1.) For an understanding of the process, it is desirable to estimate the amount of feed coal carried out of the reactor from the slurry drier bed. To fill this need, we have developed a petrographic method for determining the feed coal content of samples of dust collected from the cyclone. The method was developed on samples obtained when the pilot plant was operating on lignite, but it should also be applicable to samples from the processing of other ranks of coal.

If the dust collected from the cyclone were composed of material from only two sources and the two components differed in character, it would be possible to estimate their relative proportions from the elemental composition or other test property of the sample and its two sources. This situation would also apply in effect if some test property were sufficiently uniform among all sources but the one of interest. This is not the case here, as shown by analyses of typical bed samples from the different stages of the reactor (Table 1). Table 1 also shows that the cyclone dust is much finer than the samples of source materials, as might be expected. One should, therefore, analyze corresponding fines fractions of the source materials if this approach appeared fruitful. However, note that the composition of the fines elutriated from a particular bed may differ from the composition of particles of the same size range sampled from the bed. Thus, one can only surmise, from the composition data of Table 1, that the amount of feed coal in the cyclone dust is probably between zero and 25 weight percent.

Development of Method

In the customary form of petrographic quantitative analysis for the organic components (macerals) of coal, the sample is mixed with epoxy resin and pressed in a mold to obtain a cylindrical briquet. After hardening, the briquet is sectioned and polished in a manner such that the macerals can be identified under the microscope (ASTM Methods D2797 and D2799) (1). Using an eyepiece with crosshairs, successive areas of the polished surface are examined, and the macerals that appear under the crosshair intersection are counted. (A crosshair grid with multiple intersection points can also be used.) The number of counts of each component is proportional to its area in the section and its volume in the sample; with a sufficient number of counts, the percentage of counts for a component is a satisfactory measure of its volume percent in the sample. Points appearing on mineral matter and the resin matrix are ignored. The volume percent of each maceral on the mineral-matter-free basis is customarily reported, but can be converted to an ash- or mineral-matter-containing basis by calculation from ash content and estimated densities.

We concluded that application of this method to the cyclone fines would be very difficult because of the nature of some of the components other than the coal feed.

As gasification progresses the particles become increasingly porous and the proportion of mineral matter increases. Mineral matter other than iron sulfides is sometimes difficult to distinguish from the mounting medium, and clay particles especially are subject to plucking during the grinding and polishing. Instead we investigated a variant procedure in which we gravimetrically determine the weight percent of the sample in the briquet and, by a point count analysis, determine the volume percent of feed coal in the briquet, lumping all other components and mounting medium together. The densities of the feed coal and of the briquet are then needed to convert the volume percent of feed coal in the briquet to weight percent. From the weight percents of feed coal and sample in the briquet we obtain the weight percent of feed coal in the sample.

Some extra care in the mounting procedure is required to obtain briquets of known and uniform sample content. The usual technique in which the sample-resin mixture is pressed in a mold is not applicable because the clearances of the mold may allow liquid resin and some of the small particles to escape and thus change the composition of the mixture and resulting briquet. For this reason, we limit the sample content to obtain a mixture that is easily mixed and that will retain a minimum of air bubbles after hand stirring with a wooden splint. Note that the presence of bubbles is not deleterious provided they are uniformly distributed. Removing the bubbles by centrifuging, for example, is likely to cause sample concentration. Stirring with a propellor stirrer is satisfactory if done without breaking the surface of the mixture.

The density of the briquet can be determined very simply by weighing it in air and in water. Determining the appropriate density of the feed coal is not so simple. True (solid phase) density is easily determined by helium or water displacement or can be estimated from the hydrogen and ash content (3). However, some coals, especially high volatile C bituminous rank and lower, contain a substantial volume of submicroscopic pores. The density we use should include these pores but not those that are visible under the microscope, such as shrinkage cracks in lignite and the lower ranks of subbituminous coals. Particle density determined by mercury displacement is suitable if most of the particles are larger than about 100-mesh sieve size and if they do not contain an appreciable volume of microscopically observable pores or cracks. On our cyclone fines we determined true density by helium displacement on a Beckman Air Pycnometer; from this and porosity obtained from an equilibrium moisture determination, we calculated particle density. Note that use of this porosity value on our dried lignite feed is based on the conclusion, from unpublished work at IGT, that the dried lignite does not swell appreciably when immersed in water. However, we need to apply a correction to the pore volume because of the enhanced density of water (or actually of the water-coal complex) in the pores of low rank coal (4). This is the reason that density determined by water displacement on low rank coals is higher than density determined by helium displacement. Later we realized that if we had used apparent density in water, no correction would be necessary as the effect then cancels out. The respective equations for the particle density,  $d$ , of dry coal are -

$$d = [1/(d_{He} + 0.10) + M/(100 - M)]^{-1} \quad 1)$$

and

$$d = [1/(d_w) + M/(100 - M)]^{-1} \quad 2)$$

where  $d_{He}$  and  $d_w$  are densities in  $\text{g/cm}^3$  determined by helium and water displacement, respectively, and  $M$  is the weight percent of equilibrium moisture. The quantity 0.10 in the first of these equations is our value for the difference between the two densities for this coal (2).

In the point count analysis of the briquet the feed coal is recognized principally by the low reflectance of its vitrinite and exinite, ranging below about 0.4%, compared with the substantially higher reflectance of vitrinite that has been heated to  $800^\circ$

to 900°F in the first stage of hydrogasification and to even higher temperatures in succeeding stages. However, some particles darken as gasification progresses in the later stages; perhaps these particles contain dispersed clay that becomes more concentrated and thus lowers the reflectance. However, these particles also become grainy, so they can still be distinguished from the feed coal rather easily. We have not been able to distinguish whether particles composed of inertinite only or mineral matter only originate from the feed coal or from one of the reaction stages. Accordingly, we count as feed coal the points falling on any maceral or on mineral matter if the particle that the point is on contains any recognizable vitrinite. Then, to correct for the presence of particles from the feed coal containing inertinite or mineral matter only, we analyze by point count the fines of the feed coal that pass a 100-mesh USS sieve to obtain the volume fraction of such particles.

The weight percent of coal in the cyclone sample is calculated according to the formula -

$$\text{Coal, wt \%} = \frac{100 dV}{d_b(1 - I_c)W} \quad 3)$$

where  $d$  is the particle density of the coal,  $d_b$  is the density of the sample briquet,  $V$  is the determined volume percent of coal in the sample briquet,  $I_c$  is the volume fraction of particles in the coal fines containing inertinite or mineral matter only, and  $W$  is the weight percent of sample in the sample briquet.

#### Apparatus and Procedures

The sample was dried enough that the retained moisture did not interfere with the curing of the epoxy resin. Weighed amounts of epoxy resin, sample, and activator were mixed to yield a briquet of accurately known and uniformly dispersed dry sample content of 30 to 40 weight percent. After curing in a mold overnight the density of the briquet was determined by weighing in air and water, and the briquet was ground and polished according to the methods of ASTM D2797 (1). Feed coal briquets were prepared in the same way.

For the point count analysis a Zeiss Universal microscope was used with a 40X Achromat objective giving a magnification of 625X with a 12.5X eyepiece. Points were counted at the corners of a Whipple disk to a total of 1000 on each of two briquets. Points were counted on the feed coal fines in the same manner except that inertinite and mineral matter were also counted.

Equilibrium moisture was determined according to a modification of ASTM D1412 (1) in which a 10 g sample was used and the temperature was maintained near room temperature by placing the equilibrium vessel in an insulated box.

#### Results and Conclusions

The helium density of the feed coal fines was 1.63 g/cm<sup>3</sup> and the equilibrium moisture content 21.1 weight percent; these give a particle density of 1.18 g/cm<sup>3</sup>. The point count analysis of six briquets of the feed coal is shown in Table 2; two briquets each were prepared from three different coal-resin mixtures. The average content of vitrinitic particles (from the six analyses) was 91.0 volume percent. The amount of feed coal found in each briquet by the point count analysis, when calculated according to this average content of vitrinitic particles and expressed as percent of the amount determined gravimetrically in our preparation, ranged from 90% to 112% with an average of 102%.

Replicate determinations on some cyclone dusts (Table 3) indicates the repeatability that was obtained in the point count. Only one resin-sample mixture was prepared for each sample because of the limited quantity of sample available; for two of

them only one briquet could be made. A new section of each briquet was exposed by regrinding and repolishing to obtain a duplicate point count analysis of each briquet.

The good average recovery on the feed coal briquets lends support to the principles of the method and indicates that systematic errors have been reduced to a satisfactory level.

With the analysis for feed coal in the cyclone dust in hand we can attempt to draw some additional conclusions about the source of the remainder of the dust. For example, if we take the analyses in Table 1 to be representative of the fines elutriated from each bed, then about 45% to 55% of the cyclone dust must come from the steam-oxygen gasifier. However, note that sampling of such streams at about 1200 psi presents severe difficulties and the analyses shown may not fully represent the composition (or size distribution) of the actual process solids.

#### Acknowledgments

This work was conducted as part of the HYGAS<sup>®</sup> coal gasification program jointly sponsored by the United States Energy Research and Development Administration (ERDA) and the American Gas Association. This program is under the technical direction of Mr. Stephen C. Verikios of ERDA (now DOE) and Dr. Ab Flowers of the American Gas Association.

#### References

1. American Society for Testing and Materials, 1974 Annual Book of ASTM Standards, Part 26, "Gaseous Fuels: Coal and Coke; Atmospheric Analysis." Philadelphia, 1974.
2. Institute of Gas Technology, "Pipeline Gas From Coal - Hydrogenation (IGT Hydrogasification Process)," Project 8907 Interim Report No. 2 for the Period July 1974 to June 1975, No. FE-1221-144, pp. 286-90. Washington, D.C.: U.S. Energy Research and Development Administration, July 1976.
3. Institute of Gas Technology, "Preparation of a Coal Conversion Systems Technical Data Book," Project 8964 Final Report for the Period October 31, 1974 to April 30, 1976, No. FE-1730-21, Section PMa.44.1.2. Washington, D.C.: U.S. Energy Research and Development Administration, 1976.
4. Institute of Gas Technology, "Preparation of a Coal Conversion Systems Technical Data Book," Project 8979 Quarterly Status Report for the Period May 1 to July 31, 1976, No. FE-2286-4, pp. I-1 to I-15. Washington, D.C.: U.S. Energy Research and Development Administration, November 1976.

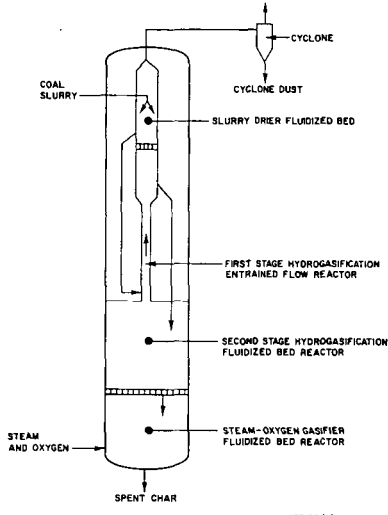


Figure 1. SCHEMATIC DIAGRAM OF HYGAS<sup>®</sup> PILOT-PLANT REACTOR  
SHOWING FLOW OF SOLIDS

Table 1. TYPICAL COMPOSITION OF SOLIDS IN THE HYGAS REACTOR  
DURING RUN 37 ON LIGNITE

	Feed Coal (Lignite)	After First Stage*†	Second Stage Bed†	Spent Char From Steam- Oxygen Gasifier†	Cyclone Dust
			wt%		
<b>Proximate Analysis (as received)</b>					
Moisture	17.0	3.7	2.6	7.0	2.6
Volatile Matter	35.2	19.2	8.5	9.3	15.5
Ash	9.7	22.9	28.2	46.1	36.5
Fixed Carbon	38.1	54.2	60.7	37.6	45.4
<b>Ultimate Analysis (dry basis)</b>					
Carbon	61.9	62.8	65.2	44.9	52.9
Hydrogen	4.31	2.70	1.56	0.94	2.00
Nitrogen	1.01	1.02	0.55	0.22	0.67
Sulfur	0.86	0.48	0.17	0.10	0.38
Ash	11.74	23.76	28.93	49.58	37.52
Oxygen (by difference)	20.18	9.24	3.59	4.26	6.53
<b>Sieve Analysis, USS</b>					
Retained on No.					
12	11.0	2.5	6.5	0.1	0.0
20	23.6	11.5	19.6	2.9	0.0
30	11.1	6.7	9.7	4.4	0.6
40	10.3	6.3	10.7	6.4	0.6
60	14.9	13.4	16.9	16.5	2.1
80	6.9	7.4	8.4	11.4	2.5
100	2.8	5.5	4.3	7.6	3.5
200	8.3	16.9	13.2	19.7	24.7
325	4.1	15.4	7.2	12.5	30.9
Pan	7.0	14.4	3.5	18.5	35.1

\*Sampled from the spouting bed above the lift line reactor.

†Because of high-pressure sampling difficulties, these analyses may not be representative of the composition or size distribution of the process solids.

Table 2. ANALYSIS OF FEED COAL

<u>Briquet No.</u>	<u>1A</u>	<u>1B</u>	<u>2A</u>	<u>2B</u>	<u>3A</u>	<u>3B</u>
Density of Briquet, g/cm <sup>3</sup>	1.216	1.210	1.198	1.198	1.209	1.209
Feed Coal in Briquet, as Prepared, wt %	33.7	33.7	28.8	28.8	26.5	26.5
Point Count Analysis						
Vitrinitic Particles, vol % of Briquet	28.5	31.9	29.9	27.2	24.6	27.1
Vitrinitic Particles, % of Whole Coal	88.8	92.1	94.0	91.0	92.1	91.2
Whole Coal, wt % of Briquet*	30.2	34.0	32.2	29.2	26.2	28.9
Whole Coal by Point Count/Whole Coal by Gravimetric Preparation, %	90	101	112	102	99	109

\*Based on average vitrinitic particle content of whole coal = 91.6 vol %.

Table 3. ANALYSIS OF CYCLONE DUSTS

<u>Sample No.</u>	<u>Briquet No.</u>	<u>Feed Coal Content, wt %</u>		
		<u>Initial</u>	<u>Reground</u>	<u>Average</u>
1	1013	5.0	4.4	4.7
2	1015	8.2	6.3	6.6
	1016	5.7	6.0	
3	1014	5.8	4.5	5.2
4	1005	2.9	3.2	4.4
	1008	6.6	5.0	
5	1007	6.6	6.6	7.1
	1009	7.1	8.1	
6	1011	7.8	8.5	8.0
	1012	7.1	8.6	
7	1006	7.0	7.3	7.8
	1010	9.3	7.4	

Developments in Solid State NMR and Potential  
Applications to Fuel Research \*

Alex Pines and David E. Wemmer

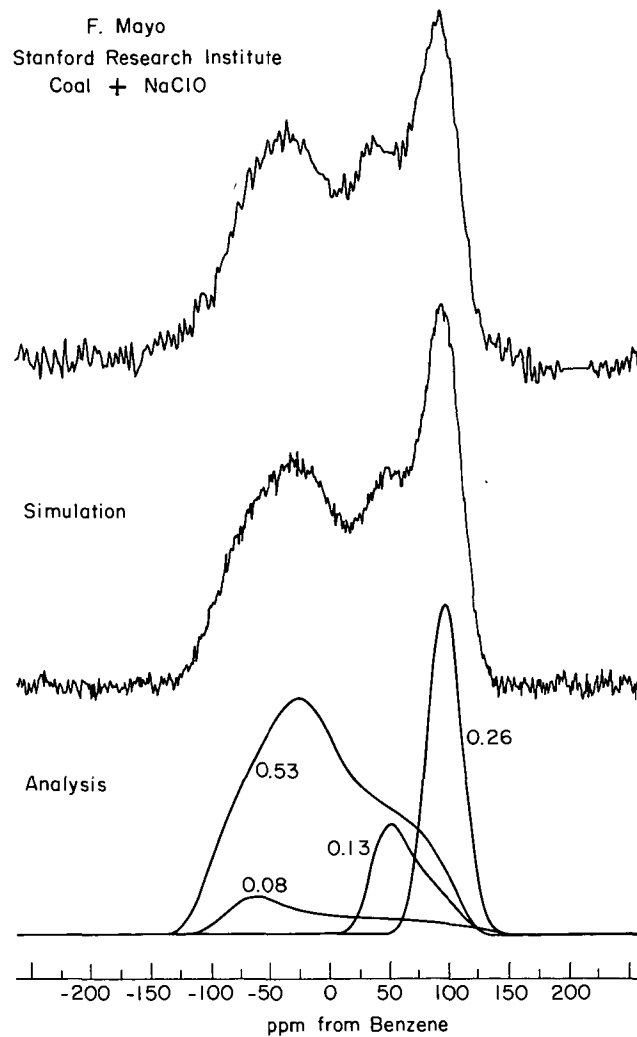
Department of Chemistry and Materials and Molecular Research Division,  
Lawrence Berkeley Laboratory, University of California  
Berkeley, California 94720

The high resolution NMR of two important nuclei ( $^{13}\text{C}$  and  $^2\text{D}$ ) in the solid state is now a practical possibility. This adds a useful tool to the arsenal of analytical chemistry in the area of solid materials which are insoluble or otherwise not amenable to classical spectroscopic techniques. The study of  $^{13}\text{C}$  is made possible by a double resonance method (Proton Enhanced NMR) due to Pines, Gibby and Waugh and has now reached the stage where analysis of some functional groups in coal is possible. A simple physical picture of the method will be given in the talk. As an example, Figure 1 shows spectra on our spectrometer and our computer from a sample of coal from Dr. F. Mayo at SRI working on an ERDA fossil energy related project. At top is the  $^{13}\text{C}$  proton enhanced NMR spectrum. At bottom are the computer generated lineshape analyses for four carbon types (aliphatic 26%, ether 13%, aromatic 53% and polycondensed aromatic 8%). In the center is the computer simulation done by adding the four shapes at the bottom and adding some noise--you must agree that there is some similarity with the experimental spectrum. We thus believe the method is quick and reasonably reliable (~ 10%) for studying whole coals, coal processing, coal by-products and other fuel related materials. We shall show several examples of this in the talk and discuss the advantages and limitations of the method.

The study of  $^2\text{D}$  NMR in the solid adds a new possible dimension since isotopic labeling during processing could be followed directly in the solid state. This was considered until recently a particularly nasty nucleus since  $^2\text{D}$  linewidth are typically 200 KHz ( $\sim$  1000 ppm wide) in the solid state. A method due to Vega, Shattuck and Pines (Fourier Transform Double Quantum NMR) now brings this nucleus into the realm of high resolution and the possibility of analytical applications. Again, a simple physical picture of the method will be presented in the talk. As an example, Figure 2 shows the first resolution of deuterium chemical shifts in the solid state. At top is an NMR free induction decay taken by the double quantum method. The Fourier transform spectrum at the bottom shows true  $^2\text{D}$  chemically shifted lines, one due to the COOD and one due to HDO. Several recent examples of this solid state  $^2\text{D}$  spectroscopy will be described and its possibilities and limitations discussed.

---

\* Supported by U.S. Energy Research and Development Administration.



XBL 773-8219

Figure 1

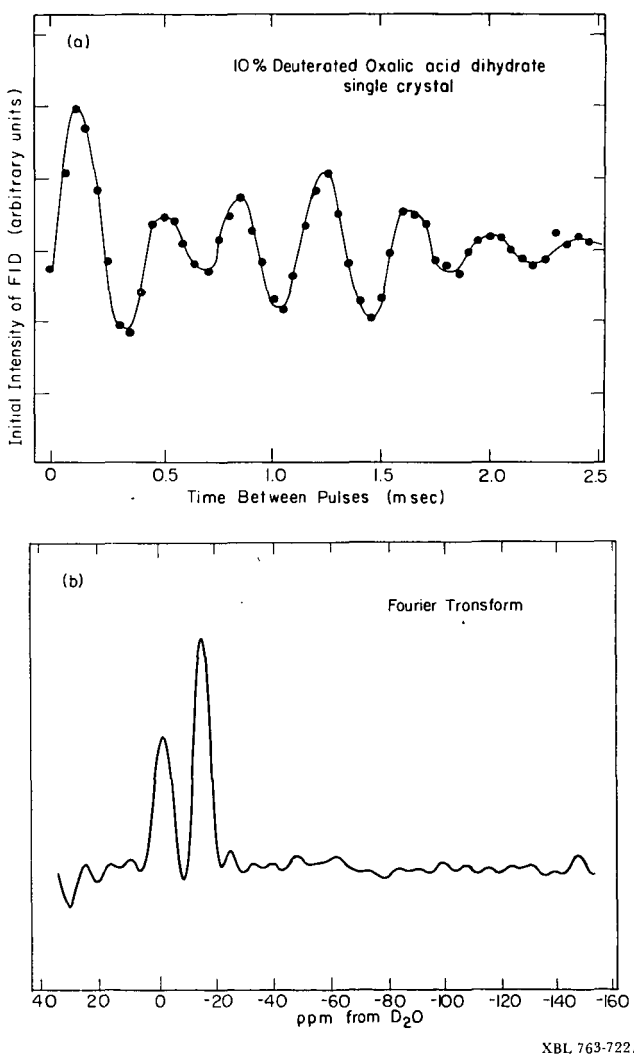


Figure 2

## <sup>13</sup>C NMR Studies of Coals and Oil Shales

Victor J. Bartuska and Gary E. Maciel  
Department of Chemistry, Colorado State University  
Fort Collins, Colorado U.S.A. 80523

and

Francis P. Miknis, Laramie Energy Research Center  
U.S. Department of Energy  
Laramie, Wyoming 82070

### INTRODUCTION

The "standard" <sup>13</sup>C nmr techniques, including pulse Fourier transform (FT) approaches<sup>1</sup> have not been generally useful for solid samples because of (1) the excessive line broadening due to dipole-dipole interactions between <sup>13</sup>C and <sup>1</sup>H magnetic dipoles, (2) chemical shift anisotropies (different shielding values for the many different orientations of the molecules in an amorphous state with respect to the magnetic field direction), and (3) long <sup>13</sup>C spin-lattice relaxation times ( $T_1$ ).<sup>2</sup> All of these problems are eliminated in liquids (or in the case of long  $T_1$  values, at least greatly reduced) by the normal tumbling motions occurring randomly in the liquid state.

For an analytical technique in the field of fossil fuels, the constraint to liquid samples has been very restrictive. For many types of samples, e.g., oil shales and typical coals, only a small fraction of the organic substances can be extracted from a solid under mild conditions that would be expected to retain the primary structural integrity of the organic compounds.

The recently developed techniques used to narrow the lines of <sup>13</sup>C nmr signals in solids are high power <sup>1</sup>H decoupling<sup>3</sup> and magic-angle spinning.<sup>4-7</sup> The former involves irradiation of the proton manifold at the <sup>1</sup>H resonance frequency. It is analogous to the common "spin-decoupling" technique for eliminating splittings due to indirect spin-spin coupling in standard high-resolution nmr experiments; but it requires much higher radio frequency power, because direct dipolar <sup>13</sup>C,<sup>1</sup>H interactions are much larger than indirect <sup>13</sup>C,<sup>1</sup>H coupling constants.

The importance of magic-angle spinning is that rapid sample spinning at the magic angle eliminates the effects of chemical shift anisotropy, *i.e.*, averaging the resonance positions corresponding to the various orientations of a particular type of carbon atom in the solid sample to the isotropic limit that would be observed if the sample were in a nonviscous liquid state.<sup>7,8</sup> This is because the anisotropic part of the shielding tensor involves a trigonometric factor which vanishes at a value 54.7° (the magic angle) for the angle between a shielding tensor axis and the magnetic field axis.

The remaining source of line broadening expected of  $^{13}\text{C}$  resonances in solid fuels is the dispersion of (isotropic) chemical shifts of a given class of carbon atoms over a range due to subtle structural differences associated with the complex structural variations in such samples. This dispersion of chemical shifts is not removed by the techniques discussed in this paper, and is ultimately a genuine source of structural information.

The third problem mentioned above, the long spin-lattice relaxation times in solids, is circumvented by the development by Waugh and coworkers of cross polarization methods, or Proton Enhanced Nuclear Induction Spectroscopy.<sup>3</sup> In cross polarization an enhanced  $^{13}\text{C}$  magnetization is achieved at a rate much faster than the rate of reestablishment of an equilibrium  $^{13}\text{C}$  magnetization via  $^{13}\text{C}$  spin-lattice relaxation. This is achieved by the  $^1\text{H}$  spin-lock procedure<sup>3</sup> and the establishment of Hartmann-Hahn conditions,  $\gamma_{\text{C}}\text{H}_1^{\text{f}} = \gamma_{\text{H}}\text{H}_1^{\text{f}}$ , where  $\gamma_{\text{C}}$  and  $\gamma_{\text{H}}$  are the magnetogyric ratios of  $^{13}\text{C}$  and  $^1\text{H}$ , respectively.

Although several variations of the general type of cross polarization experiment have been suggested, the form employed in this work is that originally described by Pines, Gibby and Waugh<sup>3</sup> for  $^{13}\text{C}$ ; it is shown schematically in Fig. 1. The key feature responsible for the success of the cross polarization experiment for  $^{13}\text{C}$  in solid samples is the rapid transfer of magnetization from the proton spin set to the  $^{13}\text{C}$  spin set under the Hartmann-Hahn condition. This transfer permits the establishment and repetitive reestablishment of the  $^{13}\text{C}$  spin polarization needed for  $^{13}\text{C}$  nmr detection, without waiting the long times (three to five  $^{13}\text{C}$   $T_1$ 's) required for establishment of the polarization via normal  $^{13}\text{C}$  spin-lattice relaxation processes. The experiment can be repeated after waiting for the protons to repolarize (three to five  $^1\text{H}$   $T_1$ 's). This repolarization is generally a much more efficient process than  $^{13}\text{C}$  repolarization by spin-lattice processes.

Using the cross-polarization/high-power  $^1\text{H}$  decoupling technique,  $^{13}\text{C}$  spectra of the type shown in Fig. 2 were obtained. A variety of factors preclude using spectra obtained in this way directly for the quantitative determination of the aliphatic carbon/aromatic carbon ratio. These factors include chemical shift anisotropies and related peak overlaps, unequal cross-polarization efficiencies and the undetermined distribution of relevant proton relaxation times. This current limitation can be eliminated only by overcoming or characterizing these factors, a subject of continuing research in these laboratories. Nevertheless, we have observed a very interesting and useful correlation obtained directly from the raw spectra.

In the spectra of the type shown in Fig. 2, the region to the right (higher shielding) of the arbitrarily-drawn vertical dashed line can be identified largely with the resonances of aliphatic carbons, while the region to the left is associated mainly with aromatic carbons (perhaps some olefinic carbons and carbonyl carbons). If the area under the spectrum to the left of the line is referred to as A, the area to the right as B, and the total area (A+B) as C, then A/C is roughly the fraction of total organic carbon that is aromatic and B/C

is roughly the fraction which is aliphatic. Then, if P is the percent (by weight) organic carbon in the sample, measured independently (by total carbon minus carbonate and bicarbonate), the quantity AP/C is an indication of the percent aromatic carbon in the sample and BP/C is the percent aliphatic carbon. Figures 3 and 4 show the results of plotting these fractions against oil yield (gal/ton). For the twenty oil shales and kerogens examined in this study, the total organic carbon content (P) ranged from 11 to 81 percent (by weight) and the (apparent) fraction of aliphatic carbon (B) ranged from 0.37 to 0.85.

Fig. 3 indicates that there is little correlation between the amount of aromatic carbon in an oil shale and its oil yield. By contrast, Fig. 3 shows a high level of correlation between the amount of aliphatic carbon in an oil shale and the yield of oil obtained in retorting. These results support the thesis that it is the aliphatic part of the kerogen that is largely responsible for the oil retorted from oil shale. The results are also consistent with earlier evidence that higher H/C ratios in oil shales are associated with higher oil yields.<sup>10</sup> Furthermore, the results suggest that refined <sup>13</sup>C nmr measurements (faster and more accurate) may provide a convenient method for determining not only the structural characteristics of kerogen, but also the economic potential of individual shales.

Similar experiments on a wide range of coal samples are underway and will be described in the talk. The resolution of aromatic and aliphatic carbons can be improved from what is shown in Fig. 2 by magic-angle spinning. The consequences of this improvement are also discussed.

#### Acknowledgement

The authors gratefully acknowledge support of this research by the U.S. Energy Research and Development Administration, Laramie Energy Research Center, and valuable discussions with Drs. J. Schaefer, E.O. Stejskal and D.L. VanderHart.

#### References

1. T.C. Farrar and E.D. Becker, "Pulse and Fourier Transform NMR," Academic Press, New York, 1971.
2. J.A. Pople, W.G. Schneider and H.J. Bernstein, "High-resolution Nuclear Magnetic Resonance," Ch. 3, McGraw-Hill, New York, 1959.
- 3a. A. Pines, M.G. Gibby and J.S. Waugh, 1972, *J. Chem. Phys.*, 56, 1776.  
b. A. Pines, M.G. Gibby and J.S. Waugh, 1973, *ibid.*, 59, 569.
4. I.J. Lowe, 1959, *Phys. Rev. Letters*, 2, 285.
5. H. Kessemeier and R.E. Norberg, 1967, *Phys. Rev.*, 155, 321.
6. E.R. Andrew, 1971, *Prog. Nucl. Magn. Reson. Spectrosc.*, 8, 1.

7. V.J. Bartuska, G.E. Maciel, J. Schaefer and E.O. Stejskal, 1977, Fuel, 56, 0000.
- 8a. J. Schaefer, S.H. Chin and S.I. Weissman, 1972, Macromol., 5, 798.
- b. E.O. Stejskal, J. Schaefer, J.M.S. Heiris and M.K. Tripodi, 1975, J. Chem. Phys., 61, 2352.
9. D.L. VanderHart, H.L. Retcofsky, Fuel, 1976, 55, 202.
- 10a. F.P. Miknis, A.W. Decora, and G.L. Cook, Pulsed Nuclear Magnetic Resonance Studies of Oil Shales - Estimation of potential oil yields. U.S. Bureau of Mines, RI 7984 (1974).
- b. E.W. Cook, Fuel, 1974, 53, 16.

#### Figure Captions

- Figure 1. Timing sequence of  $^1\text{H}$  and  $^{13}\text{C}$  irradiation and  $^{13}\text{C}$  observation in a typical cross polarization experiment.
- Figure 2. Cross polarization spectra of three oil shales with different aliphatic C/aromatic C ratios. The arbitrary vertical line roughly separates the aliphatic from the aromatic regions of the spectra.
- Figure 3. A plot of the apparent percent aromatic carbon (AP/C) of twenty oil shales and kerogens vs. the oil yields of the oil shales in gal/ton.
- Figure 4. A plot of the apparent percent aliphatic carbon (BP/C) of twenty oil shales and kerogens vs. the oil yields of the oil shales in gal/ton.

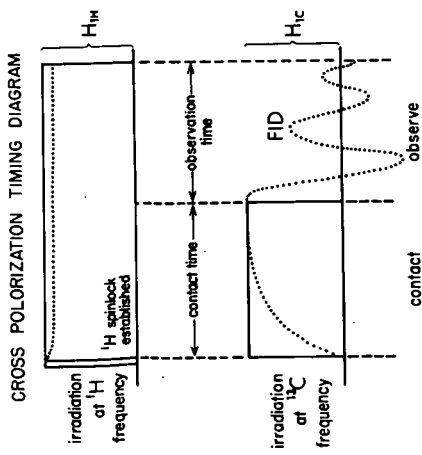


**Fig. 1**

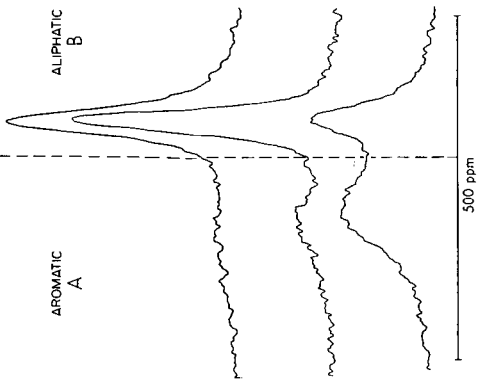


**Fig. 2**

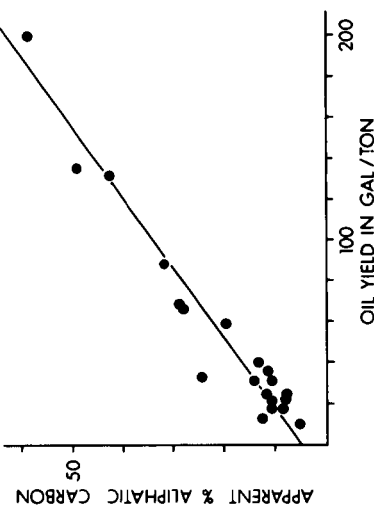


**Fig. 4**

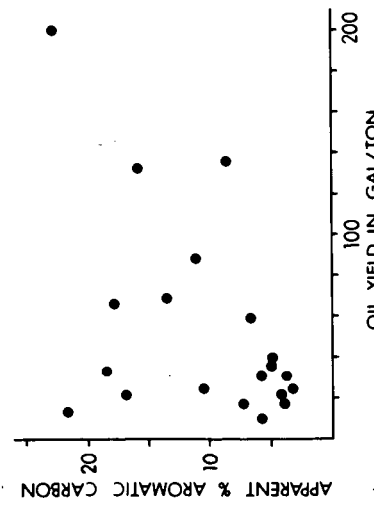


**Fig. 3**

## A CARBON-13 NMR INVESTIGATION OF THE CHEMICAL COMPOSITION OF COAL DERIVED LIQUIDS

Ronald J. Pugmire, Kurt W. Zilm, David H. Bodily  
David M. Grant, Hironori Itoh, Susumu Yokoyama

Departments of Chemistry, and Mining, Metallurgy and Fuels Engineering  
University of Utah, Salt Lake City, Utah 84112

The recent increased importance of coal as an energy source has dictated that more knowledge be obtained about the basic molecular properties of the solid and its conversion properties. Starting as early as 1966, Carbon-13 NMR spectroscopy has been employed on a limited basis for the analysis of coal derived liquids as well as petroleum samples. Extensive C-13 NMR work has been carried out in our laboratories on Utah coal derived liquid samples which have been subjected to LC and GPC separation techniques. NMR data taken at 25 MHZ and 75 MHZ have been analyzed on the acidic, basic, and neutral portions of the oils in question. These data have demonstrated that valuable chemical information can be readily obtained on aromatic and hydroaromatic ring structures and ring substituents in coal liquids obtained from different sources. The chemical significance of these results will be discussed.

### I. Introduction

The recent increased importance of coal as an energy source has dictated that more knowledge be obtained about the basic molecular properties of the solid and its conversion products. In the solid form, coal does not readily lend itself to a detailed molecular characterization. However, recent advances in experimental techniques<sup>1</sup> have been quite encouraging and promise to shed new light on this chemical structural characteristic of solid hydrocarbons.

Starting with the work of Friedel and Retcofsky,<sup>2,3</sup> Carbon-13 nuclear magnetic resonance has been employed on a limited basis for the analysis of coal derived liquids as well as petroleum samples.<sup>2,4</sup> Early works were somewhat hampered in these investigations due to such complicating factors as: 1) instrument sensitivity and techniques; 2) the lack of an extensive reservoir of Carbon-13 magnetic resonance (CMR) data on which to base detailed spectral interpretation; and 3) the extremely complex chemical composition of the materials under investigation. The problems associated with adequate instrumentation for the analysis of complex hydrocarbon investigation have largely been overcome in the past 5-7 years with the advent of fourier transform NMR techniques.<sup>5</sup> Many early workers in the CMR field concentrated their efforts on hydrocarbons and by the early 1970s a fairly extensive body of chemical shift data on fossil fuel derived hydrocarbons was emerging.<sup>6</sup> Advances in instrumentation has significantly aided in this interpretation of the composition of complex hydrocarbon mixtures. Whereas, early studies were concerned with such problems as aromaticity of various coal samples<sup>2,3,4,6,7,8</sup> and average molecular parameters,<sup>9</sup> only limited progress was made in increasing the sophistication of the analytical results obtained by means of CMR. More recent workers focused on analysis of the extracts from coal.<sup>10,11</sup> However, recognition of the necessity to fractionate coal derived liquids in order to enhance sample analysis has provided useful new information regarding the chemical structure of the liquid.<sup>12,13</sup> While LC and GPC separation schemes required to fractionate the coal liquids are well known, they involve significant effort.

This work is the first in a series describing the chemical information derived from the LC and GPC chromatographic separation and CMR analysis of the liquefaction products of Hiawatha high volatile bituminous coal.

## II. Experimental

### A. Liquefaction and Separation Procedure

The coal used in this study was Utah high volatile bituminous B rank. The details of the hydrogenation procedure have been given elsewhere.<sup>14</sup> The coal hydrogenation product was initially obtained as a "light liquid" and "heavy liquid" product in the two condenser units of the reactor. The heavy coal hydrogenated product was separated into saturates, monoaromatic, diaromatic, triaromatic, and polyaromatic/polar fractions using gradient elution through dual-packed (silica gel-alumina gel) absorption columns according to the technique described by Hirsch et al.<sup>15</sup> Further separation of these fractions was obtained by means of gel permeation chromatography (GPC) in accordance with the procedure of Haines and Thompson.<sup>16</sup> The separation scheme employed is portrayed in Figure 1.

### B. NMR Procedures

Proton spectra for each sample was obtained on a Varian EM-390 spectrometer. Carbon-13 NMR spectra were obtained on Varian XL-100 and SC-300 sepctrometers, operating in the fourier transform mode. At 25 MHZ, an 8K spectra was obtained on each sample using 0.8 sec. acquisition time, a 45° pulse angle and no pulse delay. At 75 MHZ, a 16 K spectra was obtained utilizing 0.9 sec. acquisition time, a 45° pulse angle, and no pulse delay. Deuterochloroform was used as solvent and samples were run in 5 or 10 mm tubes, depending on quantity of sample available. Standard broad-band decoupling was used and no attempts were made to compensate for differences in carbon NOE or T<sub>1</sub> values.

## III. Results and Discussion

The distribution of materials derived from gradient elution through silica-alumina gel columns are given in Table 1. The asphaltene and oil samples were further separated by GPC techniques into seven subfractions. The acidic fraction was further separated by both GPC and LC techniques into five GPC and five LC fractions. The CMR data of selected fractions of the saturate, monoaromatic, diaromatic, triaromatic, poly/polar aromatic and asphaltene fractions are shown in Figures 2-10. It was noted that in GPC fraction number one of all aromatic species, the saturates region is dominated by the spectral lines associated with normal paraffin groups. With subsequent fractions one observes a marked decrease in unbranched paraffinic structure with little or no evidence of such side chains in the last fractions (smallest molecular size) eluted from the column. These results can be rationalized by considering the volume occupied by flexible alkyl substituents on the aromatic rings in question, which, on the basis of effective molecular size, would be quickly eluted from the column.

By closely examining the spectra of each GPC fraction and comparing the line positions with those of model compounds, it is possible to derive structural features which can be used to arrive at types of molecular species that may be present. For instance, comparison of Figure 4 with Figure 6, 7, 9 and 10 illustrates that only a restricted number of possible aliphatic and/or cycloaliphatic structures are present in substantial amounts in the smaller molecular weight fractions of the polynuclear aromatic and asphaltene compounds as compared with

the monoaromatic family of compounds. In fact, the banding structure in the aliphatic region of Figures 6, 7, 9, and 10 correspond to the lines predicted for hydroaromatic species that do not contain a large number of alkyl side chains on the cycloaliphatic moiety. With the exception of GPC fractions 1 and 2 of all samples examined, which have a relatively high percentage of n-alkyl side chains, one observes a general preponderance of aliphatic line patterns similar to those in Figures 6, 7, 9, and 10.

The data in Table 2-6 provide a convenient summary of the general structural features of the individual oil fractions examined. No attempt has been made to portray all the structural features that may be present nor to attempt to quantify the results. Rather, structural features are given for the most easily identified molecular species.

It is interesting to note that electronegative functional groups containing oxygen and nitrogen usually shift adjacent carbon atoms sufficiently down-field, compared to carbons which do not bear a substituent, to enable ready identification. Of the 34 GPC fractions of the oil fractions examined in detail, only 3 fractions exhibit evidence of such functional groups. GPC fraction number one in the 3-ring aromatic fraction was the only sample exhibiting carbons contained in or adjacent to an ester functional group; i.e.,  $R-C-O-C-R$ . In the case of the polyaromatic/polar fraction, GPC fractions four and seven display resonance lines indicative of the presence of ethers and/or alcohols. The functional groups could not be present in more than a few tenths percent. Hence, the CMR data suggests that the majority of the oxygen and, perhaps the nitrogen compounds as well, are not present in the oils but, rather, have probably concentrated in the other fractions (acids, bases, and asphaltenes). The CMR data does not permit comment on the presence or absence of nitrogen or sulfur species.

With the exception of GPC fractions 1, 2, and 3 of the saturates fraction, which contain almost entirely normal paraffins, the spectral lines are so complex that at 25 MHz only a small fraction of the chemical information available can be interpreted. An illustration example of the power of carbon-13 NMR techniques to simplify the problem somewhat is illustrated in Figures 11, 12 and 13. In this case the light liquid, which has not been subjected to any further separation, was examined at 75 MHz (Figure 12) with the corresponding 25 MHz spectrum (Figure 11) included for purposes of comparison. The increased field of the superconducting spectrometer not only provides a three-fold increase in line dispersion but also greatly increases the sensitivity. Hence, with this higher field one can resolve nearly all of the lines in the spectrum in Figure 11. (It is admitted that the light liquid is less complex than the GPC fractions considered in this paper but the comparison is informative). A 250 Hz plot (Figure 13) of a portion of the aromatic region in Figure 12 demonstrates the wealth of chemical information that is available in this sample. This light liquid sample has been subjected to a GC separation using glass capillary column techniques by Dr. F. J. Yang.<sup>17</sup> Using a flame ionization detector, 306 peaks in the chromatogram were resolved and measured by means of computer techniques.<sup>17,18</sup> However, only 30-40 compounds are present in significant amounts (ca. 1%). Dr. J. N. Shoolery has employed <sup>13</sup>C NMR analysis, using microsampling techniques,<sup>19</sup> to identify toluene as the most prominent component in the light liquid.<sup>20</sup> The resonance positions of toluene are marked in Figure 12.

It is interesting to point out, without further comment, that the resonance lines for alkenes are observed in nearly all GPC fractions studied.

The GPC and LC subfractions of the acid fraction were examined in detail. GPC fractions 4 and 5 were not studied due to solubility problems in a solvent suitable for CMR studies. GPC fractions 1-3 exhibited resonance lines in the aromatic region associated with phenolic and carbazolic structures. However, little significant change was observed in either the aromatic or aliphatic regions as a function of molecular size. The five LC fractions examined also exhibited aromatic lines characteristic of phenol and carbozole derivatives. However, the relative changes in resonance line patterns were quite distinct, especially in the saturate region, between the various fractions that were eluted from the column. Perhaps the most significant result is that only in sample LC-3 (the third sample collected from the column) one observes resonance lines from both ester and ether functional groups. Inasmuch as silica-alumina gel columns have functional separation characteristics, it is not surprising that such discrimination is noted.

The basic fraction was subjected to LC separation techniques only and exhibited the resonance lines in the aromatic region characteristic of pyridine type compounds and their derivatives.

The CMR data obtained demonstrates the utility of Carbon-13 NMR techniques in obtaining chemical structural information on coal derived liquids. As with any analytical technique, the detail of the information obtained is dependent, to some extent, on the sophistication of the separations scheme employed in order to reduce the number of compounds or compound types to a manageable level. However, even the most elaborate separation scheme renders individual compound identification very tedious if it must be carried out manually. Fortunately, the advent of sophisticated data processing equipment may soon allow significant progress in this area as archival files and data manipulating sub-routines replace the inadequacies of human data analysis. The status of these techniques will be discussed.

#### ACKNOWLEDGEMENTS

Support for this work was provided by the Energy Research and Development Administration through contract E(949-18)2006.

## REFERENCES

1. See for instance, M. Melring, High Resolution NMR Spectroscopy in Solids, Springer-Verlog, Berlin, Heidelberg, New York 1976. This monograph is part of the series NMR II, Basic Principles and Progress, Editors P. Diebl, E. Fluck, and R. Kosfeld.
2. R. A. Friedel and H. L. Retcofsky, Chem. and Ind., 455 (1966).
3. R. A. Friedel and H. L. Retcofsky in Coal Science, Advances in Chemistry Series 55, American Chemical Society, Washington, D. C., 1966. Page 503-515.
4. S. A. Knight, Chem. and Ind., 1020 (1967).
5. See for instance, T. C. Forror and E. D. Becker, Pulse and Fourier Transform NMR. Instruction to Theory and Methods, Academic Press, New York and London, 1971.
6. See for instance: a) H. L. Retcofsky and R. A. Friedel, Spectrometer of Fuels, edited by R. A. Friedel, Plenum Press, New York, London, 1970, p. 90-119.  
b) J. Stothers Carbon-13 NMR Spectroscopy, Academic Press, New York, London, 1972. c) G. C. Levy and G. L. Nelson, Carbon-12 Nuclear Magnetic Resonance for Organic Chemistry, Wiley Interscience, New York, London, Sydney, Toronto, 1972.
7. H. L. Retcofsky and R. A. Friedel, Anal. Chem., 43, 485 (1971).
8. H. L. Retcofsky and R. A. Friedel, 5, Phys. Chem., 77, 68 (1973).
9. D. R. Clutter, L. Petrakis, R. L. Stenger, Jr., and R. K. Jensen, Anal. Chem. 44, 1395 (1972).
10. H. L. Retcofsky and R. A. Friedel, Fuel, 55, 363 (1976).
11. J. A. Franz, J. R. Morrey, J. R. Campbell, G. L. Tingey, R. J. Pugmire, D. M. Grant, Am. Chem. Soc., Div. of Fuel Chem., Preprints, 1975, 70, No. 3, Page 12.
12. F. K. Scheveighardt, H. L. Retcofsky, and R. A. Friedel, Fuel, 55, 313 (1976).
13. R. J. Pugmire, D. M. Grant, K. W. Zilm, L. L. Anderson, A. G. Oblad, and R. E. Wood, Fuel, 56, 0000 (1972).
14. R. E. Wood and W. H. Wiser, Ind. Engng. Chem. - Process Design Dev., 15, 144 (1976).
15. D. E. Hirsch, R. L. Hopkins, H. J. Coleman, and F. O. Cotton, Anal. Chem., 44, 915 (1972).
16. W. E. Haines and C. J. Thompson, Separating and Characterizing High-Boiling Petroleum Distillates: The USBM-AI Procedure, Laramie Energy Research Center, RI 7414.
17. F. J. Yang, Varian Associates, Instrument Division, Private Communication, August 1977.
18. S. P. Cram, F. J. Yang, A. C. Brown, III, and R. N. McCoy, Preprint, 1977 Pittsburgh Conference on Analytical Chemistry and Applied Spectroscopy, Cleveland, Ohio, March 2, 1977.
19. J. N. Shoolery and R. E. Majors, American Laboratory, May 1977, page 51.
20. J. N. Shoolery, Varian Instrument Division, Varian Associates, Private Communication, September 1977.

FIGURE 1  
SEPARATION SCHEME

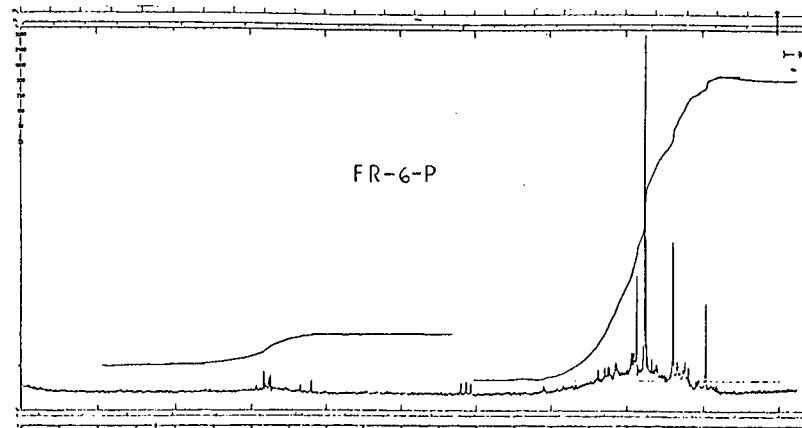
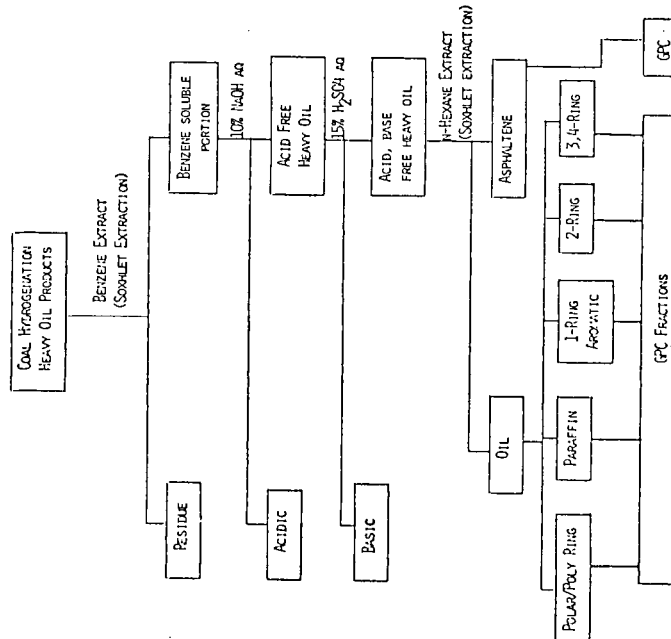


FIGURE 2 GPC subtraction number 6 of the saturates fraction of the heavy oil. UV data indicate that aromatic species are present. However, line positions in the unsaturates regional also indicate the presence of alkenes. Predominant lines are due to normal alkanes. Spectra was taken at 25 MHz.

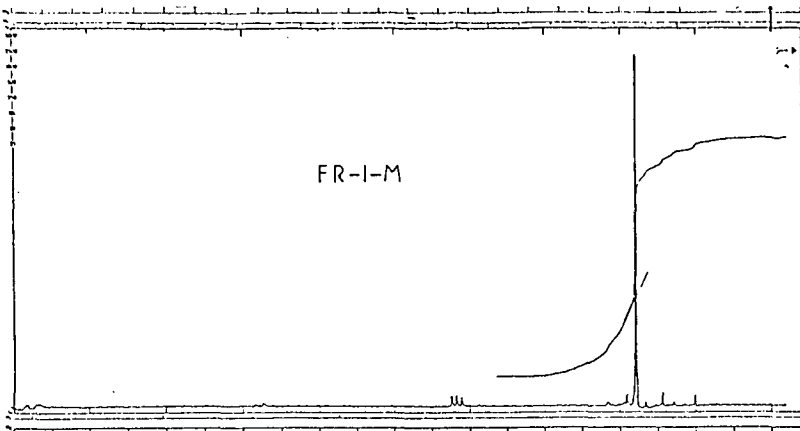


FIGURE 3 GPC subtraction number 1 of the monoaromatic fraction. Little structure is observable except in the aliphatic region where n-alkyl substituents dominate.

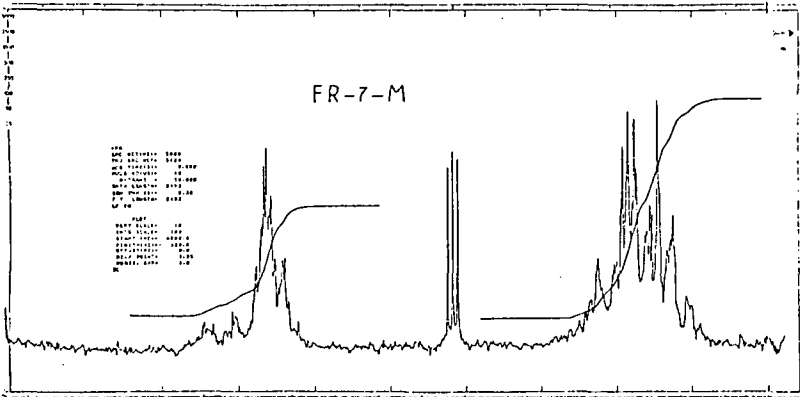


FIGURE 4 GPC subtraction number 7 of the monoaromatic fraction.

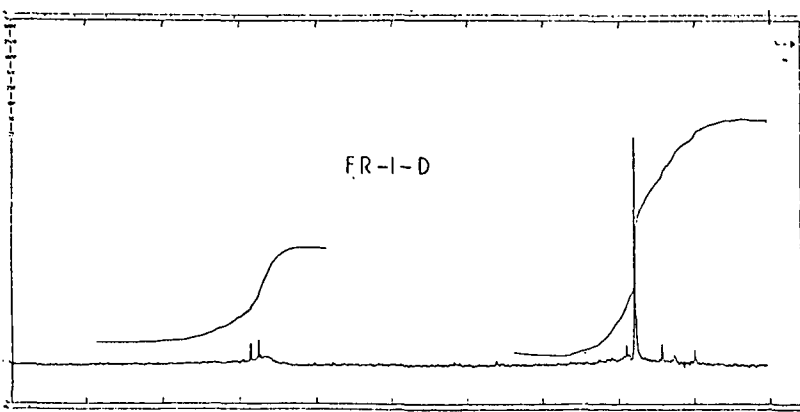


FIGURE 5 GPC subtraction number 1 of the diaromatic fraction. The structural features of the aliphatic region are dominated by n-alkyl substituents.

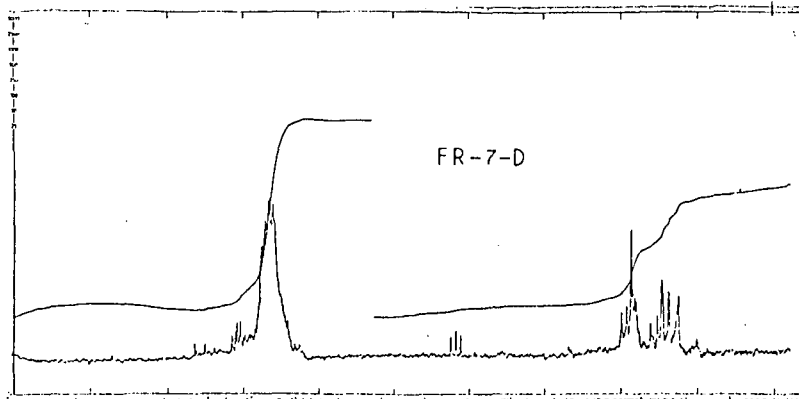


FIGURE 6 GPC subtraction number 7 of the diaromatic fraction. The aliphatic structure displays evidence of hydroaromatic species.

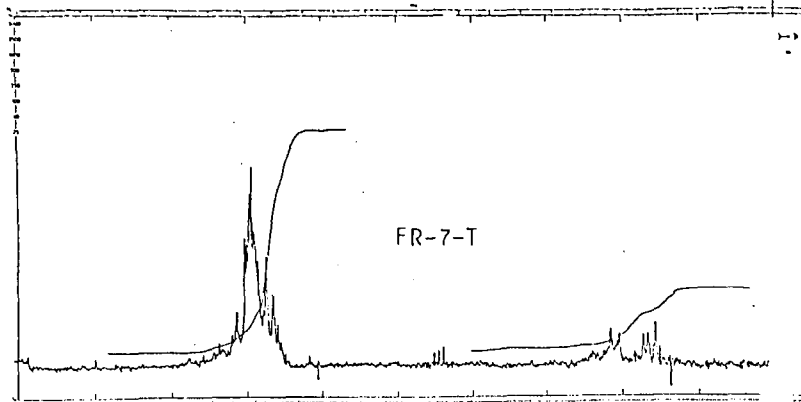


FIGURE 7 GPC subtraction number 7 of the three/four ring aromatic fraction.

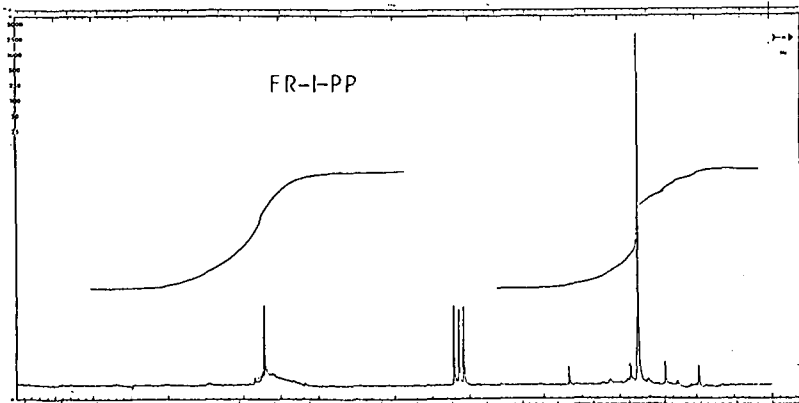


FIGURE 8 GPC subtraction number 1 of the poly/polar aromatic fraction. Note the presence of resonance lines due to n-alkyl substituents.

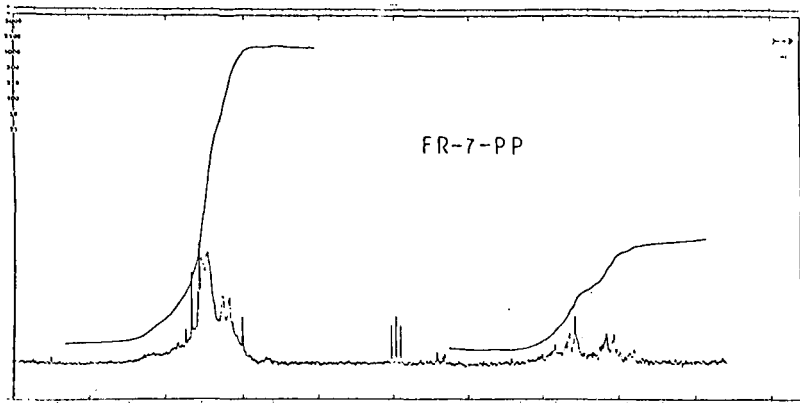


FIGURE 9 GPC subtraction number 7 of the poly/polar aromatic fraction.

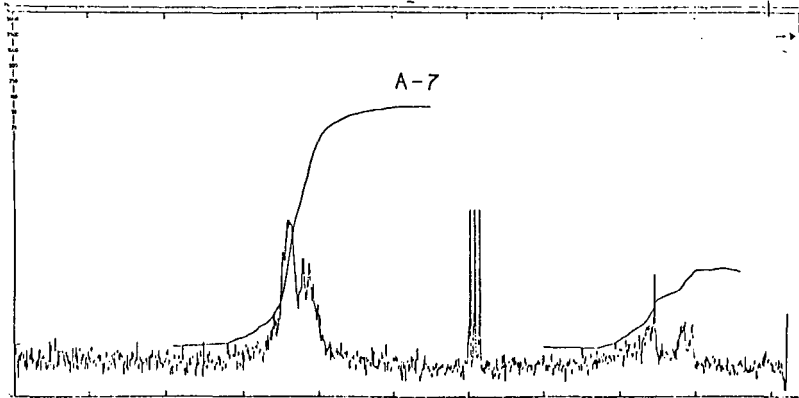


FIGURE 10 GPC subtraction number 7 of the asphaltenes. The signal to noise is too low to permit observation of minor structural features. The aliphatic region is similar to that observed in Figure 6, 7, and 9.

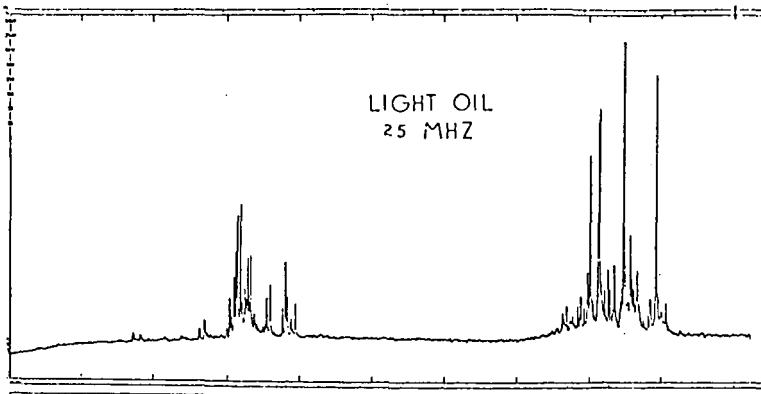


FIGURE 11 NMR spectra of light oil taken at 25 MHz. A D<sub>2</sub>O capillary was used as external lock. A total of 35,445 transients were accumulated. Total time required was 8 hours.

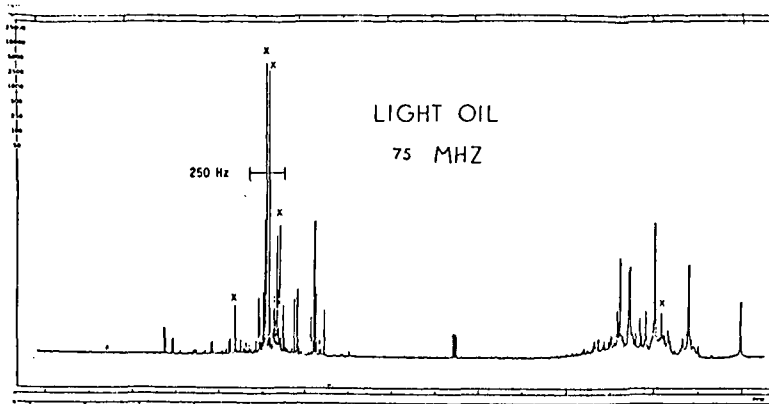


FIGURE 12  $^1\text{H}$  NMR spectra of sample shown in Figure 11. Data was taken using DCl<sub>3</sub> as an internal lock. TMS was added as a reference. The lines designated by x correspond to the lines found in toluene. Spectra width was 15 Hz. The spectra was obtained from accumulation of 203 transients requiring approximately 0.1 hour.

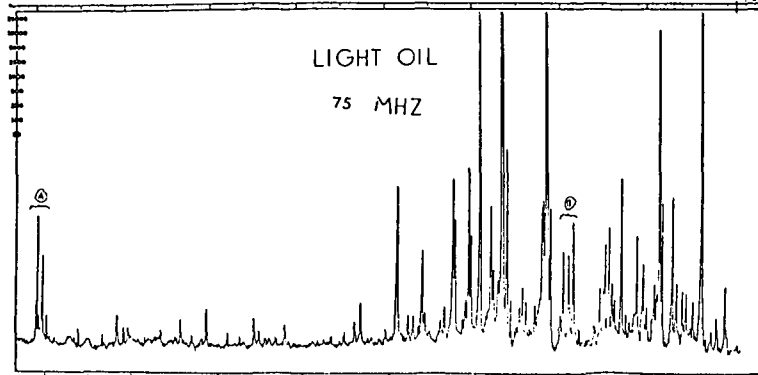


FIGURE 13 A 250 Hz region of a 4 kHz spectra taken of the aromatic region of the light oil. The spectral region is that indicated in Figure 12. 1194 transients were obtained with an acquisition time of 4.096 sec. for a total spectrometer time of 1.4 hours.

TABLE 1. DISTRIBUTION OF HEAVY OIL FRACTIONS

SAMPLE: HIAWATHA H.V. BITUMINOUS COAL

YIELD: HEAVY OIL 31.3% w/w COAL

PRODUCTS

	% HEAVY OIL	% COAL
ASPHALTENE	6	1.8
OIL	62.2	19.6
SATURATES	6.29	1.97
One-Ring Aromatic	7.76	2.43
Two-Ring Aromatic	8.05	2.52
Three-four-Ring Aromatic	8.72	2.73
POLAR/POLY RING AROMATIC	29.65	9.28
ACIDIC	12.9	4.0
BASIC	2.2	0.7
RESIDUE (BENZENE INSOLUBLE)	3.3	1.0
LOSS	12.9	4.0

TABLE 2. SUGGESTED COMPOSITION OF SATURATES FRACTION

GPC FRACTION	UNSATURATES					SATURATES						% OF OIL	
	R-C=C-R <sup>1</sup> OR AROMATICS	R-C=C*	R-C=C			$\Sigma$ -P	N	R-C=C-C-R	R-C=C	R-C=C-C*	ISO-PARAFFINS	CYCLO PARAFFINS	
FR-1-P	X					60	24	X		X		X	0.54
FR-2-P	X SIMILAR TO FR-1-P					85-90	25	MOST OF BRANCHED AND CYCLIC PARAFFIN LINES GONE					1.21
FR-3-P	X SIMILAR TO FR-1-P					85-90	24	MOST OF BRANCHED AND CYCLIC PARAFFIN LINES GONE					1.05
FR-4-P	X SIMILAR TO FR-1-P					64	18				X	X	1.09
FR-5-P		X	X			16-50	14			X	X	X	1.12
FR-6-P	X			X	X	20	14	OTHER THAN N-PARAFFINS, LITTLE DEFINITIVE STRUCTURE PRESENT					1.28
												TOTAL	6.29

<sup>1</sup>These spectral lines correspond with those of nonsubstituted benzenes as well as long chain alkenes. UV data exhibits absorption bands characteristic of aromatic rings indicating that the separations procedure does not eliminate all aromatic material from the saturates fraction.

<sup>2</sup>%P represents the percent of normal paraffins present in the sample while X represents the number average length of the alkyl chains.

TABLE 3A  
SUGGESTED COMPOSITION OF MONOAROMATIC FRACTIONS  
UNSATURATES

GPC FRACTION						$\Sigma$ -C=C-R		$\Sigma$ -C=C-R		% OF OIL	
FR1-M	X									0.93	
FR2-M	X									1.02	
FR3-M	X	X	X	X	X	X	X			1.12	
FR4-M	X	X		X	X					1.12	
FR5-M	X	X		X	X					1.04	
FR6-M	X	X	X	X			X			1.18	
FR7-M	X	X	X	X	X	X	X	X		1.37	
										TOTAL	7.79

SUGGESTED COMPOSITION OF MONOAROMATIC FRACTIONS  
SATURATES

GPC FRACTION	$\Sigma$ -P <sup>1</sup>	N <sup>1</sup>		$\phi$ -C	$\phi$ -C-C	$\phi$ -C-C-R	$\phi$ -C-C-R		CYCLO PARAFFINS	$\Sigma$ -C=C-C	% OF OIL	
FR1-M	-60	-31	X	X	X	X	X				0.93	
FR2-M	A	>10	X			X	X				1.02	
FR3-M	15-20	-8	X	X	X	X	X				1.12	
								BROAD BAND RICH IN STRUCTURE				
FR4-M	A	-5	X		BROAD BAND WITH LITTLE STRUCTURE						1.12	
FR5-M	A	-5	X		BROAD BAND WITH MUCH BRANCHED AND CYCLIC ALIPHATIC STRUCTURE						1.04	
FR6-M	A		X	X					X	X	1.18	
FR7-M	A		X						X	X	1.37	
											TOTAL	7.79

<sup>1</sup>Same as N in Table 2 except in the aromatic fractions N is used to designate the n-alkyl substituents.

<sup>2</sup>Not measured.

TABLE 4  
SUGGESTED COMPOSITION OF DI-BIATIC FRACTIONS

FPC FRACTION	UNSATURATES						SATURATES						% OF OIL
	R-C=C	C-C=C-R	C-C=C-R				$\Sigma n-p^1$	n <sup>1</sup>			CYCLOPARAFFINS		
FR-1-D							25	13					X 0.95
FR-2-D	X	X	X	X	X	X	-	5	X	X	X	X <sup>2</sup>	0.22
FR-3-D		X	X	X	X	X			X	X	X	X <sup>2</sup>	1.02
FR-4-D		X	X	X	X	X			X	X	X	X <sup>2</sup>	1.12
FR-5-D		X	X	X	X	X			X	X	X	X <sup>2</sup>	1.14
FR-6-D		X	X	X	X	X			X	X	X	X <sup>2</sup>	1.34
FR-7-D		X	X	X	X	X			X	X	X	X <sup>2</sup>	1.23
												TOTAL	8.02

<sup>1</sup>See Footnote 2 in Table 2.

<sup>2</sup>Decreasing amounts as molecular weight decreases.

TABLE 5  
SUGGESTED COMPOSITION OF 3-RING AROMATIC FRACTIONS

FPC FRACTION	UNSATURATES						SATURATES						ISO- PARAFFINS	% OF OIL
	R-C=C	C-C=C-R					$\Sigma n-p^1$	n <sup>1</sup>						
FR-1-T	X	--SINGS WITH NO RESOLVABLE STRUCTURE--					16	9	X	X	X		X 1.21	
FR-1-T	X	X	X			X	-				X	X	X 1.27	
FR-3-T	X	X	X	X	X					X	X	X	X 1.15	
FR-4-T	X	X	X	X	X					X	X	X	X 1.41	
FR-5-T	X	X	X	X	X	X				X	X	X	X 1.57	
FR-6-T	X	X	X	X	X					X	X		X 1.05	
FR-7-T	X	X	X	X	X					X	X	X	X 1.15	
													TOTAL 8.74	

<sup>1</sup>See Footnote 2 in Table 2.

TABLE 6  
SUGGESTED COMPOSITION OF POLYAROMATIC/POLAR FRACTIONS

FPC FRACTION	UNSATURATES						SATURATES						$P-CH_2-OR^2$	% OF OIL
	R-C=C	C-C=C-R					$\Sigma n-p^1$	n <sup>1</sup>						
FP-1-PP	BROAD BAND OF LOW INTENSITY						25	13	X				X 4.25	
FP-2-PP	X	X	X	X	X	X	-	5	X	X	X	X	X 5.02	
FP-3-PP		X	X	X	X	X			X	X	X	X	X 3.93	
FP-4-PP		X	X	X	X	X			X	X	X	X	X 3.00	
FP-5-PP		X	X	X	X	X			X	X	X		X 4.03	
FP-6-PP		X	X	X	X	X			X	X	X		X 4.22	
FP-7-PP		X			X	X			X	X	X		X 4.44	
													TOTAL 29.55	

<sup>1</sup>See Footnote 2 in Table 2.

<sup>2</sup>The resonance lines observed are probably due mainly to ethers but the line positions do not preclude the possibility of secondary or tertiary alcohols.

FIELD DESORPTION MASS SPECTROMETRY - APPLICATION TO THE ELUCIDATION OF THE STRUCTURE OF HUMIC ACID by R. L. Wershaw, U.S. Geological Survey, Denver Federal Center, Denver, CO, 80225, D. F. Barofsky and E. Barofsky, Oregon Graduate Center, Beaverton, Oregon, 97005

Progress in the elucidation of the structure of humic acids has been impeded, in part, by our inability to dissociate humic acid aggregates into analyzable units and, in part, to the nonavailability of adequate analytical tools to monitor the chemical procedures. Field desorption mass spectrometry (FDMS) has two properties that make it ideally suited to the analysis of relatively large molecular aggregates such as humic acids. These are: (1) The FDMS of most compounds exhibit predominantly molecular or pseudomolecular ions and (2) sample volatilization is not required prior to ionization.

Field desorption mass spectrometry allows us to monitor the chemical reactions that we have used to dissociate humic acid fractions by enabling us to observe the dissociated fragments. The most significant result arising out of this work to date, has been the observation of humic acid fragments following either chlorination or permethylation; in untreated samples we get no spectra. The disaggregation on permethylation is attributed to a reduction in hydrogen bonding.

The first part of this paper will present a brief survey of FDMS, that is, its theory, instrumentation, and techniques. The second part will present the results of the application of FDMS to the structural elucidation of humic acid and the general applicability of FDMS to similar problems.